lajss.org©
Latin American
Journal of Solids
and Structures
www.lajss.org

Study on the fracture behavior of tungsten alloy projectile cores under impact loading

Guixiang Yin[1] https://orcid.org/0009-0006-9133-8278,Wenbin Li[1*] https://orcid.org/0000-0003-4031-9764, Peng Chen[1] https://orcid.org/0009-0002-6810-0713,   Mingxin Zhang[2] https://orcid.org/0009-0000-4527-0088,

1. *Nanjing University of Science and Technology School of mechanical engineering, Nanjing, Jiangsu, China.*
2. *Xi'an Modern Control Technology Research Institute，Xi'an 710065, China*

Email: dzsygx@njust.edu.cn, lwb2000cn@njust.edu.cn, cp1212@njust.edu.cn, 491596634@qq.com,*

* Corresponding author

Abstract

With the increasing complexity of modern armor structures, especially the emergence of spaced targets with large angle of obliquity, tungsten alloy long rod projectiles face new penetration performance challenges. To investigate the influence of spaced targets with large angle of obliquity on the penetration performance of tungsten alloy long rod projectiles with large length-diameter ratio, this study conducted experiments and numerical simulations on the penetration of 93W long rod projectiles into oblique spaced targets. By applying high-speed camera, the fracture morphology of the long rod projectile after penetrating the target was successfully captured. In the water tank recovery experiment, the residual penetrator core of tungsten alloy rod projectile was obtained after oblique penetration, and systematic scanning electron microscopy (SEM) analysis was conducted. The results indicate that the fracture mode of the long rod projectile was mainly manifested as transgranular fracture of tungsten grains. In addition, the J-C constitutive parameters of 93W were determined, and the inherent laws of long rod projectiles penetrating multi-layer spaced targets were revealed through experiments and simulations. The study found that the mechanism of action for long rod projectiles penetrating spaced targets with large angle of obliquity was ballistic deflection and the fracture of long rod projectiles. By altering the conventional “thin-thick-thin” structure of the long rod projectiles and implementing measures such as adding nosed armor-piercing blocks and front weakening grooves, the penetration effectiveness against oblique spaced targets could be significantly enhanced.

Keywords

spaced targets with large angle of obliquity; large length-diameter ratio; fracture; long rod projectiles

Graphical Abstract

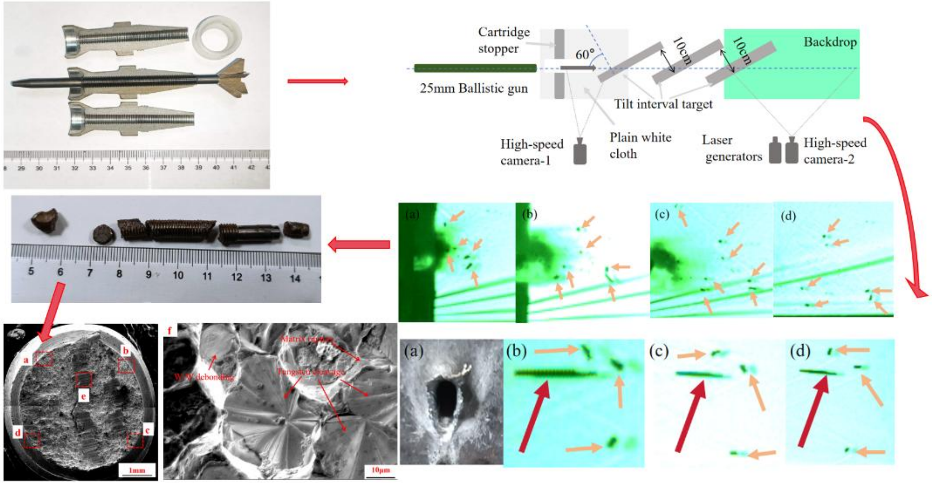

1 INTRODUCTION

The penetration process of tungsten alloy rod projectiles into homogeneous steel targets with large angle of obliquity at high speed is basically clear. It can be described as follows: in the early stage of penetration, the projectile body advances closely along the bottom of the crater, and the formed crater flanging is almost perpendicular to the advance direction of the projectile body. After the transition stage, in the later stage of penetration, the crater is the straight penetrated crater with a diameter of 1.5 times or slightly larger than the projectile diameter. The penetrator core exhibits a significant turning angle ϕ towards the normal direction of the target surface (G.Z. Zhao et al. 1992, W.B. Li et al. 2002).

Over decades, extensive research has been conducted on long-rod penetration mechanics. For instance, Anderson studied the influence of velocity on the L/D effect (Charles E. Anderson et al. 1995), the laws of long-rod projectiles penetrating targets with large angle of obliquity and full of water (Charles E et al. 1995). (Hohler V et al. 1978) carried out X-ray tests on long-rod projectiles penetrating inclined targets. Rosenberg researched the impact of yaw angle on penetration performance (Y. Vayig et al. 2021) and the formed crater diameter (Zvi Rosenberg et al. 2017). (A.J. Stilp et al. 1997, V. Hohler et al. 1995) investigated the ultra-high-speed penetration of tungsten-aluminum alloy rods and the distribution of debris clouds behind penetrating double-layer targets, and Walker (S. Chocron et al. 2023) studied the model of long rod projectiles penetrating multi-layer metal plates.

Numerous scholars have conducted a series of experiments and numerical simulation studies on layered targets; however, there are different results regarding whether the anti-penetration performance of the layered targets increases or decreases. Iqbal and Senthil observed that the ballistic limit of the monolithic target was relatively higher, followed by in-contact layered targets and spaced targets (M.A. Iqbal et al. 2017, K. Senthil et al. 2013). Zukas and Scheffler concluded from numerical research that delamination significantly weakened the anti-penetration performance of thin and medium thickness targets (J.A Zukas et al. 2001). Flores-Johnson’s research found that monolithic targets had better bullet-resistant performance than multi-layer targets made of the same material, and this effect diminished with increasing impact velocity (E.A. Flores-Johnson et al. 2011). Iqbal discovered that at a oblique angle of 30°, the ballistic limit of monolithic targets was 3% and 7% higher than that of layered and spaced targets, respectively. When the oblique angle increased to 45°, the differences among the three configurations became more pronounced. The ballistic limit of the monolithic target was increased by 10% and 24% compared to the in-contact layered targets and spaced targets, respectively. The reason behind the differences in ballistic resistance among the three configurations was the changes in the trajectory during penetration (M.A. Iqbal et al. 2017). The ballistic resistance of the targets increased with the increase of inclination for sharp-nosed projectiles, but it’s opposite for blunt-nosed projectiles (Zaid Mohammad et al. 2017, P.K. Gupta et al. 2018, P.K. Gupta et al.2017). Zaid found that when impacted at a oblique angle of 30°, the ballistic limits of monolithic and layered targets decreased by 14.36% and 12.22%, respectively (Zaid Mohammad et al. 2020). Deng et al. studied the ballistic resistance of single-layer targets, in-contact multi-layered targets and spaced Q235 steel targets, and found that the resistance ranked from greatest to least as single-layer targets > in-contact multi-layered targets > spaced targets (Y Deng et al. 2012, Y Deng et al. 2013, W. Zhang et al. 2012).

However, many other researchers have found that layering or spacing the targets has a gain effect on ballistic resistance. S. Dey conducted a study on the ballistic resistance of double-layer steel targets and found that in the case of blunt-nose projectiles, the double-layer targets could significantly enhance ballistic resistance. However, these advantages seemed to disappear when using sharp ogival-nosed projectiles (S. Dey et al. 2007). Research has found that failure modes with higher energy absorption could significantly improve the ballistic resistance of armor. By replacing monolithic targets with double-layer targets, the bending deformation of the targets could be enhanced. The double-layer targets underwent considerable deformation before fracturing, thereby improving the ballistic resistance (T Børvik et al. 2002, T. Børvik et al. 2002). Mohammad observed that for all armor-piercing bullets, contact-layered targets exhibited higher energy absorption capabilities compared to monolithic targets. Additionally, it was found that energy dissipation in both target configurations decreased when incident at an oblique angle (Zaid Mohammad et al. 2021). The ballistic resistance of the targets was significantly influenced by obliquity (J. Awerbuch et al. 1997, V. Madhu et al. 2003, D.W. Zhou et al. 2008, M. A. Iqbal et al. 2010, M.A. Iqbal et al. 2013, Z Mohammad et al. 2017). Gupta studied the ballistic resistance angles of monolithic and layered targets made of aluminum 1100-H12 when subjected to sharp-nosed projectiles at oblique incidence. With the increase in inclination, all targets exhibited enhanced ballistic limits. Furthermore, when impacted at oblique angles of 0°, 30°, and 45°, the strain energy absorbed by monolithic target material was 19%, 22%, and 28% higher than that of the layered target material, respectively (PK Gupta et al. 2017). (X. Teng et al. 2008) research showed that for dual-layer armor plates, the optimal configuration for ballistic resistance was to have the upper layer made of highly ductile and low-strength material, while the lower layer was made of less ductile and high-strength material, which helped to improve the ballistic limit. Tang et al. conducted a numerical simulation of projectiles obliquely impacting spaced target plates and found that a structure with staggered arrangements of different materials could enhance the target's penetration resistance (Tang et al. 2019). Long et al. experimentally tested the penetration power of a steel long rod projectile on multi-layer, large-spaced targets and found that as the penetration into the remaining layers continued, some material around the projectile head experienced erosion (Y. Long et al. 2004). Zhao et al. conducted a numerical simulation of a rod kinetic projectile penetrating multi-layer target plates, and the results showed that the penetrator core did not fracture. Zhao et al. found that when the angle of projectile penetration exceeded 30°, the ballistic limit of the spaced target began to surpass the ballistic limit of the equal-thickness contact target (R.Y. Zhao et al. 2012). Iqbal et al. found that the oblique impact of 7.62mm bullets on single, layered, and spaced steel plate targets resulted in ballistic deflection and ricochet (M.A. Iqbal et al. 2017). Yuan et al. simulated the oblique penetration of a long rod projectile at a 30° angle of obliquity on a three-layer spaced target, conducting analyses on speed and residual mass. The front part of the projectile eroded earlier with less stress impact, while stress concentration occurred in the middle part of the projectile, and the connection between the projectile body and the tail fins also experienced significant stress (Y. N. Yuan et al. 2011). Dong et al. conducted research on projectiles penetrating multi-layer spaced targets at different initial velocities, angles of impact, and numbers of target layers. The results indicated that, the projectile was subjected to asymmetric forces, resulting in a change in the angle of attack of the projectile after penetration(Y.X. Dong et al. 2010). Li et al. studied the penetration of long rod projectiles into dual-layer spaced targets and found that tilted front or rear plates could enhance the ballistic resistance of dual-layer spaced armor. When the front plate remained unchanged, the increase in the angle of the rear plate improved ballistic resistance (J.Q. LI et al. 2009).

Numerous researchers study the way brittle and ductile fracture occurs in different alloy materials, both macroscopically and microscopically (Jinxin Pan et al. 2025, C. Sénac et al. 2024, Maziar Khademi et al. 2024). Effect of radiation defects on grain boundary evolution under shock loading (H. Chang et al. 2024). Estimation of fracture toughness of tungsten fiber reinforced tungsten composites by H. Gietl (H. Gietl et al. 2020).

Therefore, this study has undertaken the corresponding work. In previous work, during tests with large-caliber, tungsten alloy long rod projectiles with large length-diameter ratio, it was found that penetration into a three-layer, large-spaced target resulted in the fracture of penetrator core, significantly reducing the penetrative power of the armor-piercing projectiles. Currently, the fracture mechanisms of penetrator core and the effects of spaced targets with large angle of obliquity on the penetration ability of tungsten alloy long rod projectiles with large length-diameter ratio are not yet clear. This study aims to investigate these issues from both macro and micro perspectives through ballistic experiments combined with numerical simulations. The research includes examining the effect mechanisms of oblique spaced targets on tungsten alloy long rod projectiles, the laws of tungsten alloy long rod projectile penetrating into oblique spaced targets, and the ballistic characteristics of different tungsten alloy long rod projectile structures penetrating oblique, large-spacing spaced targets. The findings will provide valuable references for future research and engineering design for subsequent researchers.

2 Penetration test

To study the influence of oblique spaced targets on the penetration capability of tungsten alloy long rod projectiles, this research employed a 25mm ballistic gun to launch test projectiles using small grain black powder and 4/7 propellant. The initial velocity of the launch was controlled by adjusting the mass of the loaded propellant. A cartridge stopper was placed in front of the target to intercept the cartridge that detached after exiting the projectile. Three-layer oblique spaced targets were configured with a 60° obliquity angle and 10 cm vertical spacing between target plate back surfaces. The experimental setup is illustrated in Figure 1. To observe the impact velocity of the long rod projectile, high-speed camera-1 was used to capture and measure the speed. For photographing the state of the long rod projectile after penetrating the target, high-speed camera-2 was used in conjunction with laser generators and a background cloth. Figure 2 shows the 93W (The 93W alloy was sourced from Xiamen Tungsten Co., Ltd. (China).) long rod projectile with a core length of 120mm, a mass of 54g, along with the three-petal aluminum cartridge, fins and nylon obturator ring, matched with the 25mm ballistic gun. All target plate materials were made of Q235 steel. The Q235 steel is a common carbon structural steel with an elastic modulus (E) of approximately 200-210 GPa, a Poisson's ratio (ν) ranging from 0.25 to 0.33, and a tensile strength of 375-500 MPa.

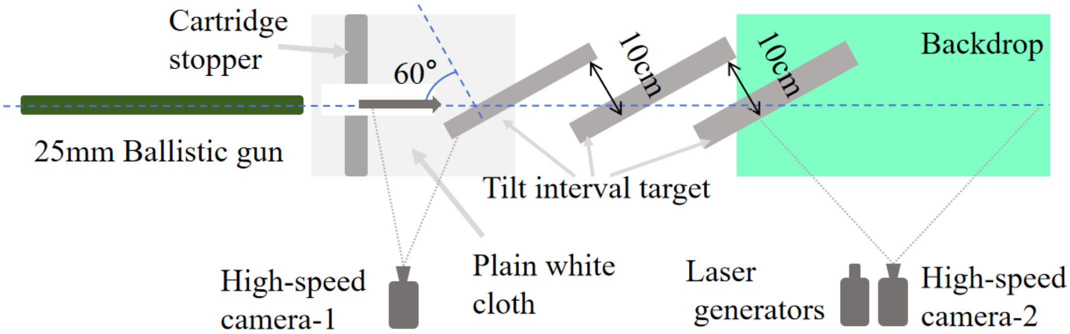

***Figure 1**. Setup of three-layer oblique spaced target.*

***Figure 2.** 93W long rod projectile.*

The experimental plan for this study is shown in the table below:

Table 1. Experimental plan.

Number	Number of layers	Targets
1	Single layer	20mm
2	Double layers	10mm+20mm
3	Three layers	10mm+20mm+20mm

2.1 Penetration into the single-layer target

Figure 3 shows the state of the penetrator core after the 93W long rod projectile penetrating vertically in the preliminary test, and it can be seen that the residual core remained intact.

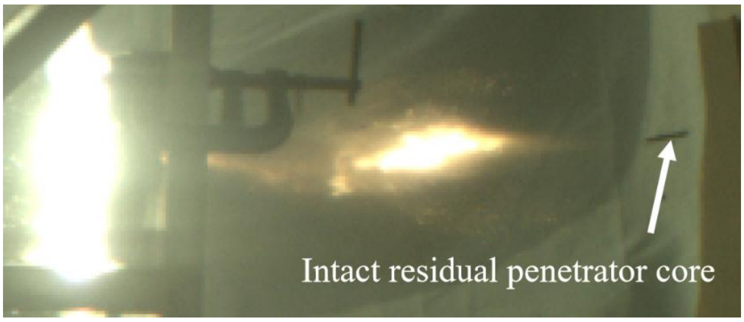

***Figure 3.** Residual penetrator core after perpendicular penetration into the single-layer target.*

As shown in Figure 4, (a) represents the target diagram after penetrating a single-layer target plate at a 60° angle of obliquity, and (b)~(d) represent the residual penetrator core diagrams captured by laser and high-speed camera.

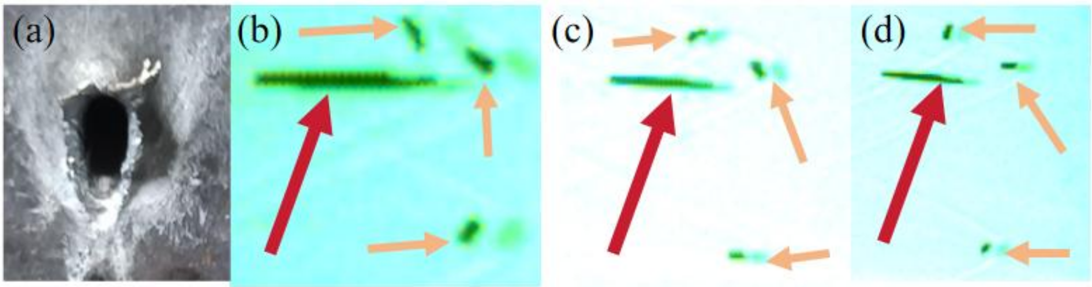

***Figure 4**. Target and residual penetrator core diagram after penetrating a single-layer target plate.*

Figure 4 shows the target and residual penetrator core diagram after a Q235 target plate with a thickness of 20mm and a oblique angle of 60 °were penetrated by a long rod projectile at a speed of 1159m/s (impact velocity). It can be observed that in approximately the front half of the target thickness, the rolling lines of the flanged target material are clearly oriented towards the front of the target. This orientation occurred during the formation of the front crater (the horn-shaped crater at the front surface of the target). Within this region, the rolling lines of the target material on the crater's slip slope tended to be tangent to the crater's bottom line, and there were marks left by the projectile body on the bottom of the slip slope. This indicated that during the penetration process in this region, the projectile body closely followed the bottom of the crater to advance. The target material above the penetrator head flipped upwards. Since Q235 steel is relatively soft, compared to the harder steels such as 603, this part of the target material would separate from the target body.

From the residual penetrator core behind the target, it is clearly visible that part of the core had broken off from the main body. The dark red arrows indicate the main body of the penetrator core, while the orange parts show the broken-off segments of the penetrator core. The overall deformation of the penetrator core was relatively small, and the fracture surface of the broken penetrator was quite smooth. Additionally, the penetrator core underwent a rotational angle. This was because when penetrating the oblique target plate, the force exerted on the projectile head during cratering and exiting the target was almost perpendicular to the core. As shown in Figure 5, the force ultimately caused the head of the penetrator core to break and the entire penetrator core to rotate. Hohler [5] found that after long-rod projectile penetrated inclined target plates, the head of the long-rod projectile was noticeably bent (often breaking into several pieces). The action of asymmetric forces caused the non-fractured front portion of the long-rod projectile to experience significant bending, with the bent long-rod projectile impacting the second target plate at a large pitch angle, significantly reducing its penetration capability. This was the main mechanism by which fixed inclined target plates resisted and eroded the long-rod projectiles.

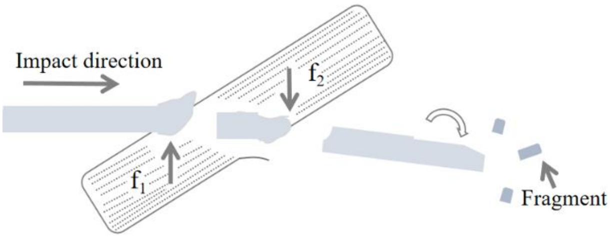

***Figure 5**. Schematic diagram of the principle of deflection and fracture of the head of penetrator core.*

2.2Penetration into the double-layer oblique spaced target

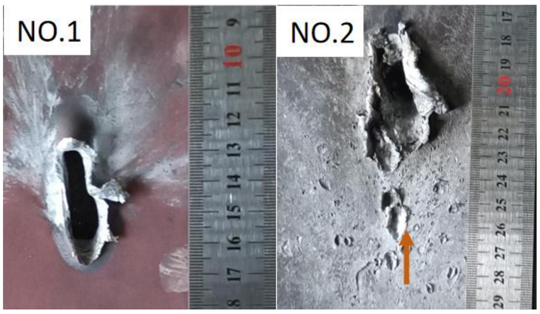

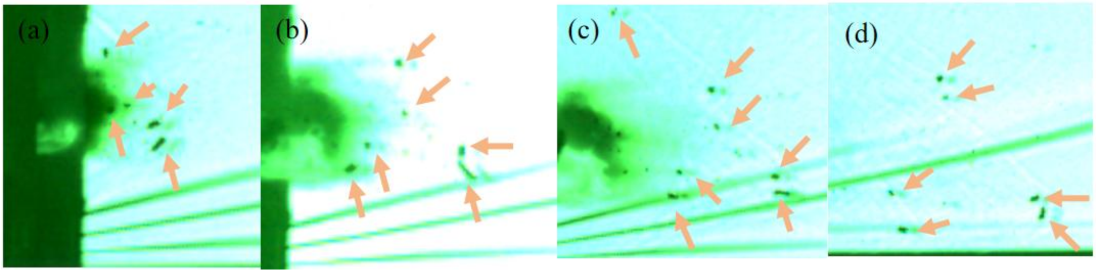

Figure 6. *The target and residual penetrator core diagram after penetrating the double-layer target.*

Figure 6 shows the target and residual penetrator core diagram after a double-layer Q235 target plate with a thickness combination of 10mm+20mm and a oblique angle of 60 °was penetrated by a long rod projectile at a speed of 1162m/s. It can be seen that there are numerous small pits on the second layer target. This was caused by the impact of fragments formed by the breaking of the head after the long rod projectile penetrated the first layer target with a thickness of 10 mm. Additionally, the craters on the second layer suggested that the penetrator core experienced rotation. After penetrating the second layer target with a thickness of 20mm, the penetrator core eventually shattered into multiple small pieces.

2.3Penetration into the three-layer oblique spaced target

Figure 7. *The target and residual penetrator core diagram after penetrating a three-layer target.*

Figure 7 shows the target and residual penetrator core diagram after a three-layer Q235 target plate with a thickness combination of 10mm+20mm+20mm and a oblique angle of 60 °was penetrated by a long rod projectile at a speed of 1395m/s. It can be seen that there are numerous small pits on the second layer of the target plate, and several shallow small pits on the third layer. This corroborates that after penetrating the two-layer target, the penetrator core broke into multiple small pieces.

2.4Penetration into the three-layer oblique spaced target Recovery of the penetrator core

After the tungsten alloy long rod projectile with large length-diameter ratio penetrating oblique targets, the penetrator core broke into multiple segments, in order to recover the residual penetrator core without damaging or contaminating the fracture surfaces during the recovery process, this study designed a plan for recovering residual penetrator core through a water medium. A water tank (50 cm × 50 cm × 100 cm) was placed 1 m behind the target to decelerate the residual projectile core. Simulation calculations confirmed that this configuration provides sufficient deceleration capability. Figure 8 shows the recovered residual penetrator core after a long rod projectile penetrated a single-layer target. (The other cross-sectional morphologies were similar, which could explain the fracture mechanism and cross-sectional morphology of 93W.)

Figure 8. *Recovered residual penetrator core through a water tank.*

Although water was used as a soft recovery medium, it could not definite whether it had no effect on the fractures of the residual projectile cores. In this study, when conducting SEM and metallographic analyses, the smaller parts of the head and tail were excluded, and the other fracture surfaces were analyzed. The results showed that the fracture surfaces were neat and exhibited similar states. Therefore, one of the fracture surfaces was selected for systematic analysis.

The recovered residual penetrator core showed a relatively neat fracture surface with minimal plastic deformation. This phenomenon differed from the test pieces and projectile bodies recovered in compression tests and penetration tests. Figure 9(a) shows an image of the residual penetrator core from a 93W penetration test, featuring a typical mushroom-shaped head. Figure 9(b) is SEM image. Prior to observation, the sample was polished using 280#, 400#, 800#, 1200#, and 1600# sandpapers, followed by polishing the surface with W5 diamond paste. The sample surface was then etched for 5-10 seconds using a tungsten alloy etchant solution (water: NaOH: K3 [Fe (CN)6] = 10:1:1), rinsed clean with alcohol, dried, and observed for its microstructure.

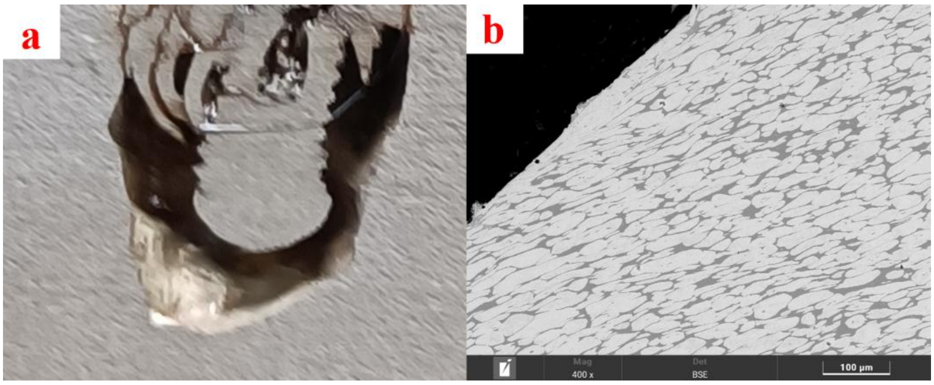

Figure 9. *Residual penetrator core and SEM image from penetration test.*

To analyze the fracture morphology of the fracture surface and determine the penetrator core fracture mechanism, the fracture surface was imaged using scanning electron microscopy (SEM), and the segmentation of penetrator core was imaged using metallography. The specimen treatment method was the same as described above. Figure 10 shows the SEM images of the fracture surface, and Figure 11 shows the metallographic images of the cross-section.

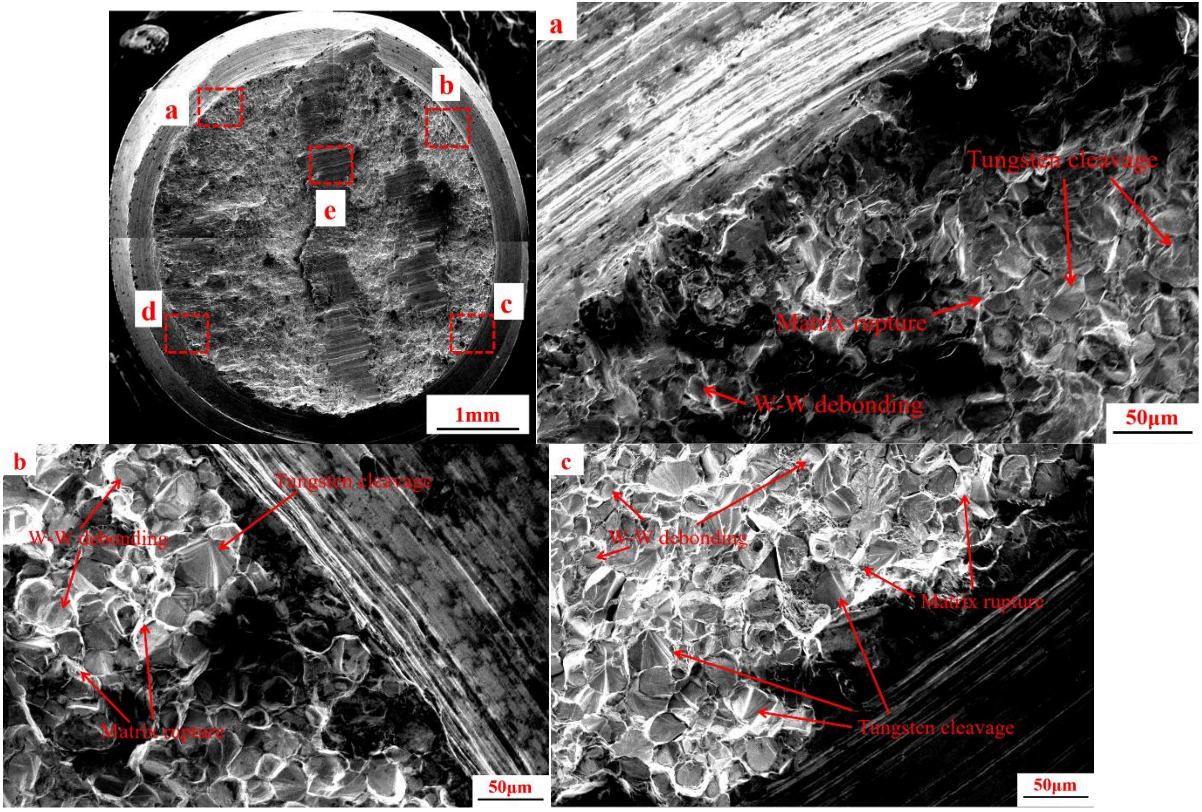

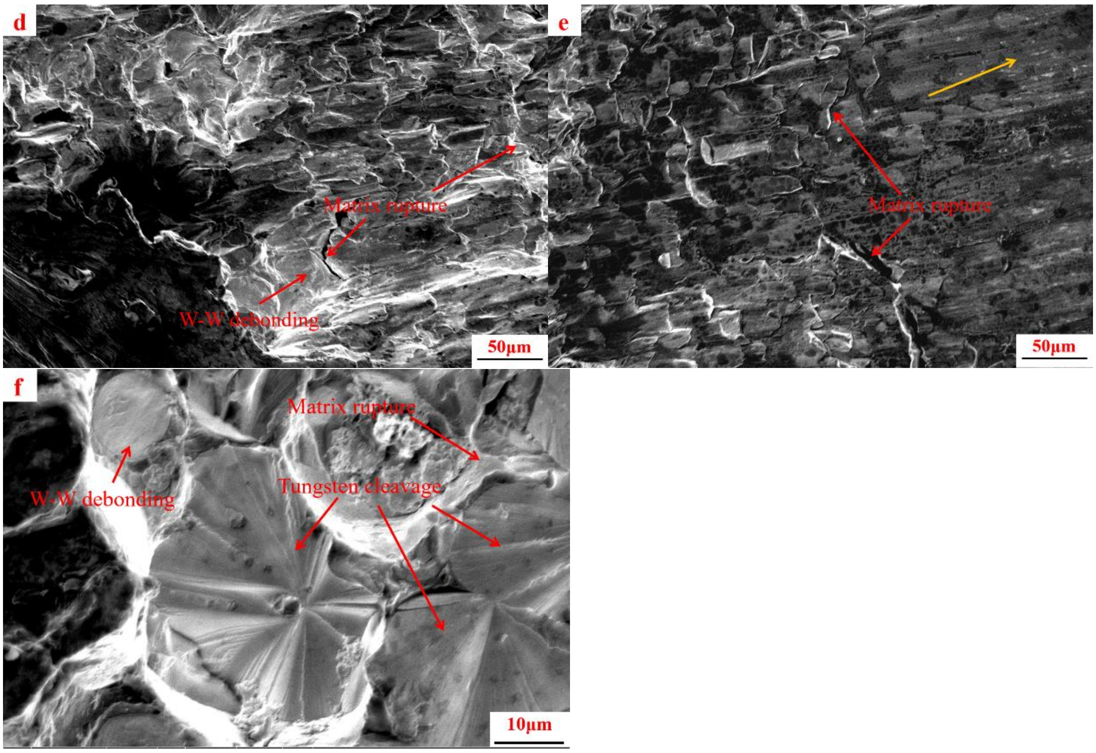

Figure 10. *SEM images of the fracture surface.*

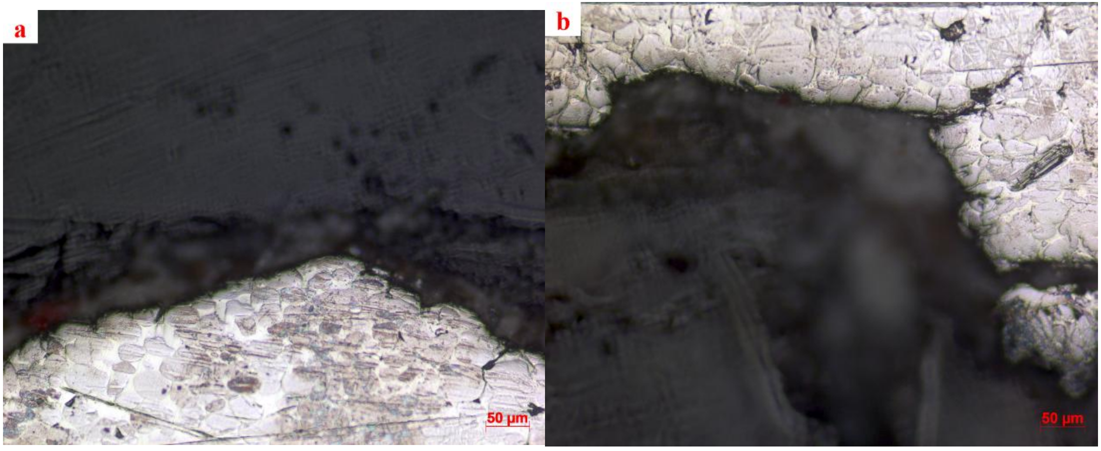

Figure 11. *Metallographic images of the cross-section.*

Comprehensive analysis of Figures 9-11 reveals the following observations. Figure 9 shows the SEM of residual penetrator head after the penetration of 93W alloy long rod projectile, where tungsten (W) grains were severely compressed, with the compression becoming more severe closer to the interface, resulting in elongated grains. In Figure 10, the fracture surface of the tungsten penetrator core showed almost no deformation, and the granular fracture surface at points a-c is clearly visible. The fracture mode was primarily transgranular, with the binder phases Ni and Fe also fracturing. W grains with dimensions ≤10 micrometers exhibited intergranular fracture, while at points d and e, W grains underwent severe deformation due to sliding and compression. Cracks formed between the W phase and the binder phase, and the binder phases Ni and Fe experienced significant deformation. The last image in Figure 10 is a close-up of fragmented W grains. Figure 11 shows the cross-section metallographic image of the fracture surface, which is transgranular fracture. These observations indicate that the W phase in the 93W alloy exhibited high compressive resistance and was not easily susceptible to failure. Under tensile and shear stresses, failure was primarily caused by transgranular fracture of the W grains. H. Safahi observed brittle fracture of tungsten wires at both room and elevated temperatures (H. Gietl et al. 2025).

3 Numerical Simulation

Through experiments involving the penetration of multi-layer oblique spaced targets by long rod projectiles, compared to previous studies on vertical penetration into semi-infinite Q235 steel (G. X. Yin et al. 2022), it was discovered that multi-layer oblique spaced targets could significantly enhance the anti-penetration capability of armor, increasing it by about one time. Due to the close spacing between target plates, it was difficult to observe the penetration process in detail using high-speed camera, and only the state of the penetrator core at a considerable distance behind the target could be observed. Therefore, finite element simulation was needed to analyze the penetration process.

3.1 Constitutive model of 93W

The Johnson-Cook (J-C) constitutive model (JOHNSON G R et al. 1983) is widely used in engineering. The original Johnson-Cook constitutive model was proposed by Johnson GR and Cook WH in 1983 and has been widely applied ever since. The J-C constitutive model is a semi-empirical model based on experimental phenomena, comprehensively taking into account the factors that influence material mechanical properties such as strain hardening, strain rate hardening, and material thermal softening effects. Its flow stress expression is as follows:

$$\sigma = (A + B\varepsilon^n)(1 + Cln\dot{\varepsilon}^*)(1 - T^{*m}) \tag{1}$$

Where ε represents the plastic strain, *A*, *B*, *C*, *n*, and *m* are material parameters, the dimensionless strain rate is expressed as $\dot{\varepsilon}^* = \dot{\varepsilon}/\dot{\varepsilon}_0$, with as the reference strain rate $\dot{\varepsilon}_0 = 1.0s^{-1}$, and the homologous temperature T^* is expressed as $T^* = (T - T_r)/(T_m - T_r)$, T_m is the melting temperature and T_r is the room temperature.

3.2 Damage model of 93W

The failure of materials is a complex physical phenomenon influenced by multiple factors. For the failure of metallic materials under higher stress, strain rate, and temperature conditions, Johnson et al. (C. Sénac et al. 2024) proposed the JC failure model, which took into account the effects of stress triaxiality, temperature, and strain rate. The model employed the accumulated damage criterion and defined the damage parameter:

$$D = \sum \frac{\triangle\varepsilon_{\mathrm{eq}}}{\varepsilon_f} \tag{2}$$

Where, $\triangle\varepsilon_{\mathrm{eq}}$ is the increment of equivalent plastic strain for a computational cycle, and ε_f is the failure strain of the material under the stress, strain rate, and temperature for the current computational cycle. When the damage parameter D = 1, material failure occurs.

The expression for the failure strain is as follows:

$$\varepsilon_f = [D_1 + D_2 \exp(D_3\sigma^*)](1 + D4\ln\dot{\varepsilon}*_{eq})(1 + D_5T^*) \tag{3}$$

Where, D_1-D_5 are material parameters; σ^* is the stress triaxiality; $\dot{\varepsilon}*_{eq}$ is the dimensionless equivalent strain rate, $\dot{\varepsilon}*_{eq} = \dot{\varepsilon}_{eq}/\dot{\varepsilon}_0$ is the actual strain rate and $\dot{\varepsilon}_0$ is the reference strain rate; T^* is the dimensionless temperature, $T^* = (T - T_r) = (T_m - T_r)$, where T is the instantaneous temperature, T_r is the reference temperature, and T_m is the melting temperature of the material.

3.3 Acquisition of Simulation Parameters

The material mechanical properties were tested through quasi-static compression tests and dynamic compression (SHPB) tests to obtain the simulation parameters for 93W. The dimensions of the quasi-static compression specimens were ɸ5mm*8mm, and the dynamic compression (SHPB) test specimens were ɸ4mm*4mm. The experimental data were calculated to obtain the true strain-stress relationship, and a Johnson-Cook parameter fitting was conducted, as shown in Figures 12-14:

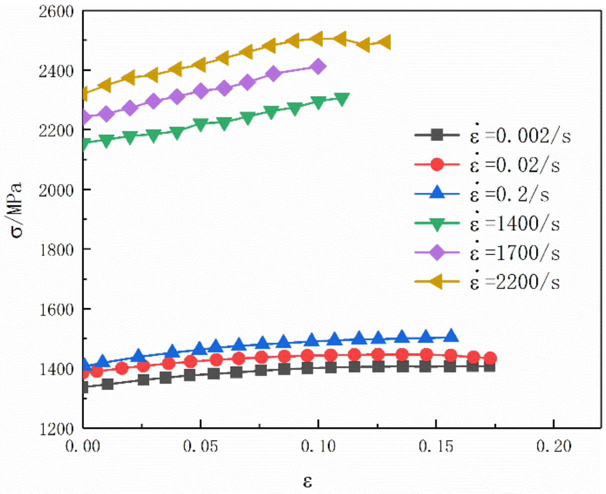

Figure 12. *Quasi static and dynamic stress-strain relationship.*

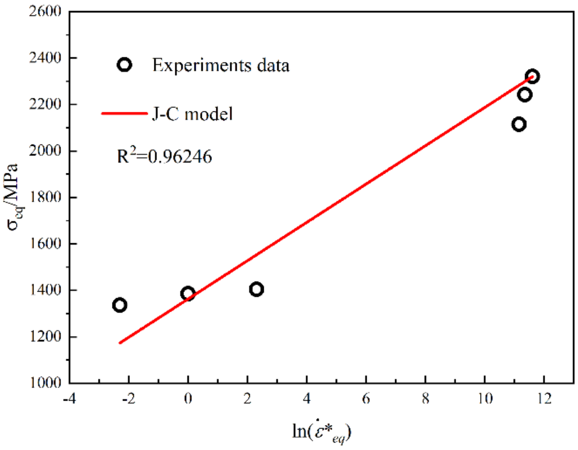

Figure 13. *Relationship between dimensionless strain rate and yield strength.*

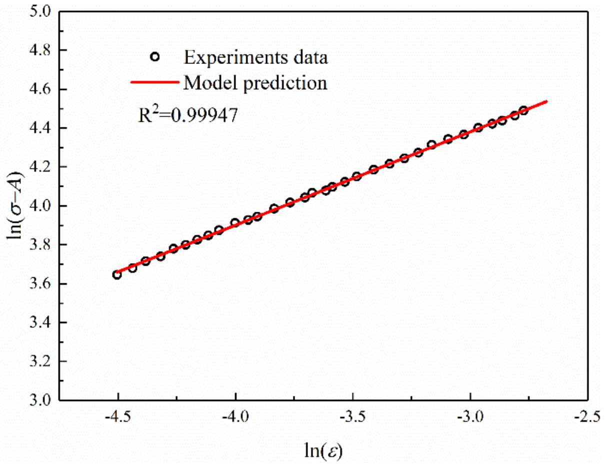

Figure 14. *Relationship between equivalent plastic strain and stress.*

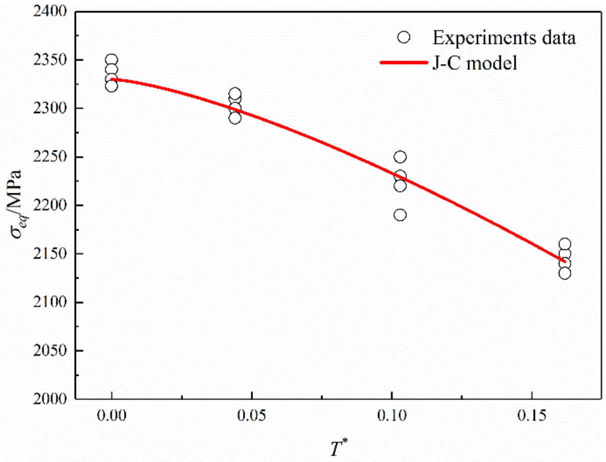

Figure 15. *The functional relationship between dimensionless temperature and yield strength*

The yield stress *A* obtained from the fitting is 1336 MPa, the strain rate coefficient *c* is 0.053, the strain hardening modulus *B* is 235, and the strain hardening exponent *n* is 0.435, The temperature index m is 1.38.

Table 2. Simulation Parameters.

	P_0/(kg/m3)	C_p/J·kg-1·K-1	$\dot{\varepsilon}_0$	A/MPa	B/MPa	n	C	m
Q235[50]	7800	469	1	410	20	0.08	0.1	0.55
93W	17600	169	0.2	1336	235	0.435	0.053	1.38
	S_1	*v*	T_r/K	D_1	D_2	D_3	D_4	D_5
Q235[50]	1.33	0.29	293	0.3	0.9	-2.8	0	0
93W[50]	1.44	0.303	300	2.0	1.77	-3.4	0	0

Numerical simulation was conducted by the finite element software ANSYS/LS-DYNA and the Lagrange algorithm. First, a simulation was carried out to assess the impact of mesh size, balancing simulation accuracy and computational time, and a mesh size of 0.5mm was ultimately selected for the projectile and target. Figure 15 shows the mesh diagram of the penetrator core model. Figure 16 illustrates the impact of mesh size on the simulation. The deviation analysis compares simulation results with experimental vertical penetration data of Q235 steel targets obtained from preliminary ballistic tests.

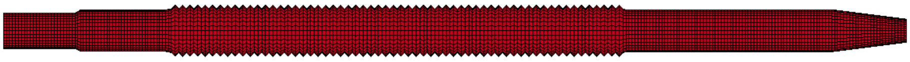

Figure 15. Mesh diagram of the penetrator core model.

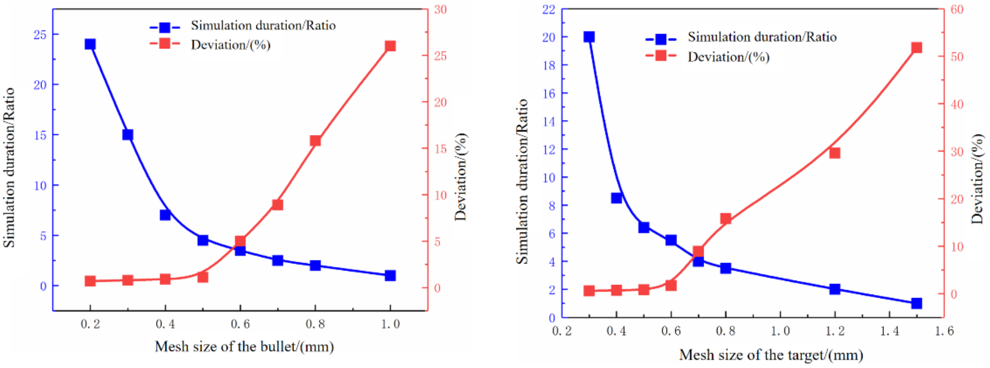

(a) (b)

Figure 16. *Effect of mesh size on the simulation.*

3.4 Simulation of experimental conditions

The following presents the numerical simulation of the experimental conditions. The results show that the penetrator core fractured neatly, and the post-perforation fragmentation pattern closely resembled the experimental results. As shown in Figure 17 (compared to Figure 4), after penetrating a single-layer target, the penetrator head fractured, while the residual part of the penetrator remained intact. As shown in Figure 18 (compared to Figure 6), after penetrating a double-layer target, the penetrator core shattered, but due to the limited simulation time, it did not disperse. In reality, the shattered penetrator core would scatter randomly under aerodynamic forces. Figure 19 (compared to Figure 7) shows the simulation of the shattered penetrator core after penetrating a three-layer target. Since the third layer target was not penetrated in the experiment, the comparison could only be made based on the final state of the third layer target. It can be seen that there are several small craters on the third layer target (Figure 19b). The experiment and simulation correspond well, allowing finite element simulation studies on the penetration of long rod projectiles into oblique spaced targets.

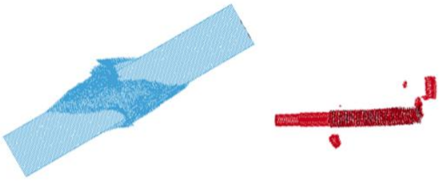

Figure 17. *Simulation result of penetrating a single-layer target.*

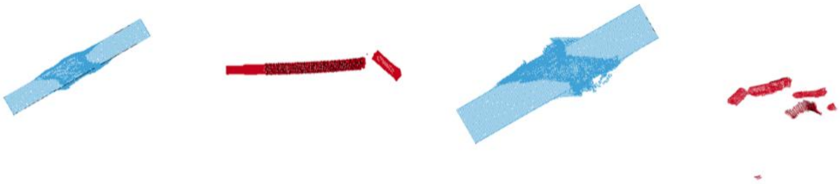

Figure 18. *Simulation result of penetrating a double-layer target.*

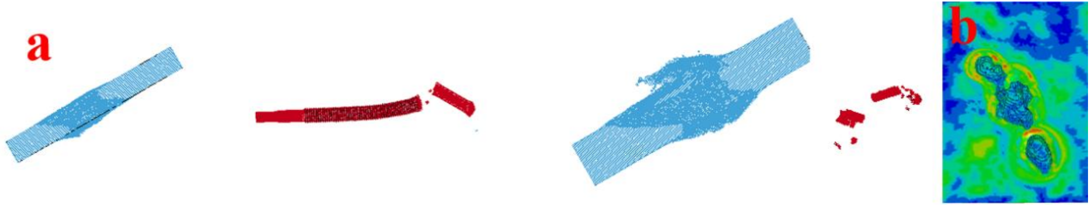

Figure 19. *Simulation result of penetrating a three-layer target.*

4 Simulation of the influence of oblique spaced targets on the penetration performance of tungsten alloy rod projectiles

To investigate the penetration law of different penetrator core structures against target plates with varying angles and spaced distances, a simulation study was conducted using the obtained simulation parameters and methods. Adjustments were made to the penetrator core structure, impact attitude, the angle, thickness, and spacing of the target, with the simulation conducted at an impact speed of 1400 m/s. The study examined the minimum target thickness that caused the penetrator head to fracture at different oblique angles; the impact of the spacing distance between the first and second layers on penetration depth after penetrating a Q235 target with single layer of 10mm and 60°angle of obliquity; and the influence of impact attitude (pitch and yaw) of the penetrator core on oblique spaced targets.

4.1 Influence of oblique spaced targets on the penetration performance of different projectile types

As shown in Figure 20, there are four projectile types, including the experimental projectile type. Type-B has a thinner threaded section compared to Type-A, and Types C and D change the length-to-diameter ratios of the penetrator core. The units in the figure are in mm. Figure 21 shows the penetration results for four types of the penetrator core structure.

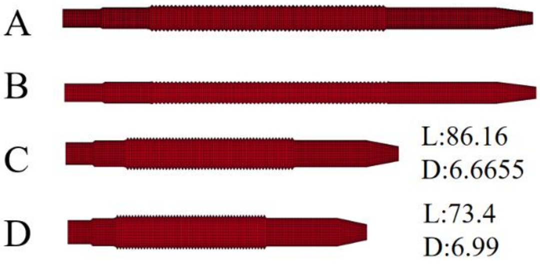

Figure 20. *Four types of the penetrator core structure.*

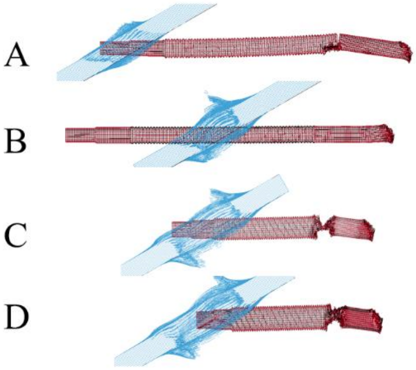

Figure 21. *Penetration results for four types of the penetrator core structure.*

Figure 21 shows the penetration results for four types of the penetrator core structure. All four types of penetrator core penetrated the 7mm thick Q235 steel plates with 60°angle of obliquity at a speed of 1400 m/s. It is evident that Type-A experienced head fracture, and Type-C and D penetrator cores with reduced length-to-diameter ratios could not effectively avoid head fracture. Comparative analysis of Type-A, C, and D penetrator cores reveals their shared thin-thick-thin structural configuration, namely a thinner front and rear with a thicker middle section. This structure is well known to enhance penetration power and flight stability while meeting the requirements for launch strength. However, this design exhibits drawbacks when the tungsten alloy long rod projectiles penetrate oblique spaced targets, making the penetrator core prone to fracture. Therefore, this study focuses on the penetration of Type-A and B projectiles into large-spaced targets with large angle of obliquity.

4.2 Target thickness causing the penetrator core fracture at different angles

Figure 22 shows the relationship between the oblique angle and thickness of the target when the penetrator core head fractures. It was found that within the large angle range of 45~70°, as the target inclination angle increased, the required target thickness for the head of tungsten alloy armor-piercing projectile to fracture after penetrating the target gradually decreased. It is generally believed that when the oblique angle of the target exceeds 70°, the armor-piercing projectile is prone to ricochet, so this angle range is not discussed here. It is clearly evident that Type-B projectile exhibited better fracture resistance compared to Type-A. For Type-A projectiles, when the oblique angle of the target was 55 °, the target thickness only needed to be slightly greater than one time the diameter of the projectile to cause the penetrator core to break. There was an approximately linear decrease in the target thickness required for the head fracture of Type-B penetrator core.

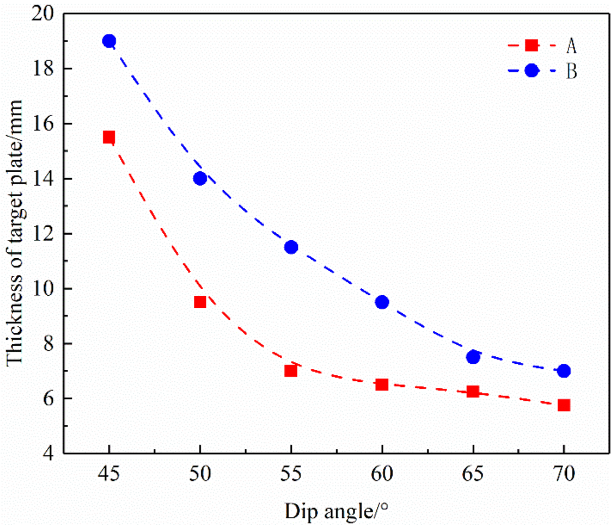

Figure 22. *The relationship between the oblique angle and thickness of the target when the penetrator core head frac*tured.

4.3 Influence of the spacing distance of the oblique target on penetration depth

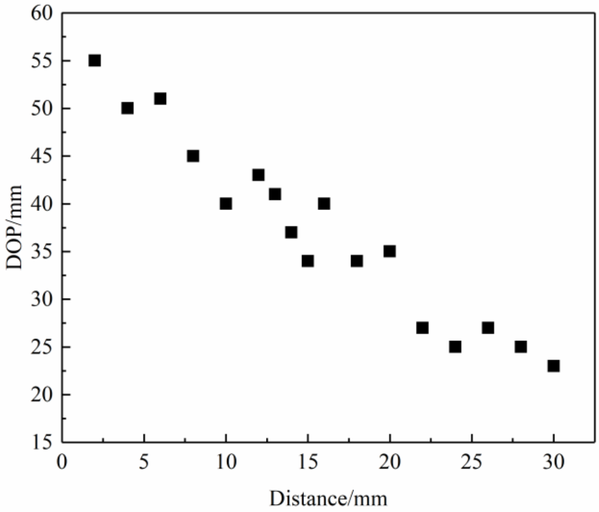

Figure 23. *Penetration depth diagram corresponding to the spacing between two layers of the target.*

Figure 23 shows the penetration trajectory depth on the second layer of the target when Type-A penetrator core penetrated a target with single layer of 10mm and 60°angle of obliquity. The distance refers to the trajectory distance between the back surface of the first layer target and the front surface of the second layer target. As the distance increased, the penetration depth showed a fluctuating downward trend. The fluctuation was caused by the fractured head reaching the second layer target first, creating a crater for the subsequent main body of the penetrator core to penetrate, thus reducing the oblique angle of the target, as shown in Figure 24. As the distance changed, the impact attitude of the fractured penetrator core changed, and the residual body after penetrator core with the fractured head cratering, affected the penetration of the subsequent penetrator core. Therefore, the combined effects resulted in a fluctuating downward trend in penetration depth.

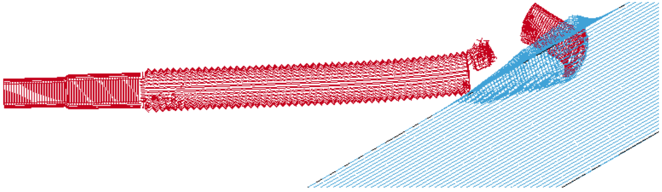

Figure 24. *Cratering of fractured head of long rod projectile.*

4.4 Influence of impact attitude (pitch) of long rod projectiles on penetration depth

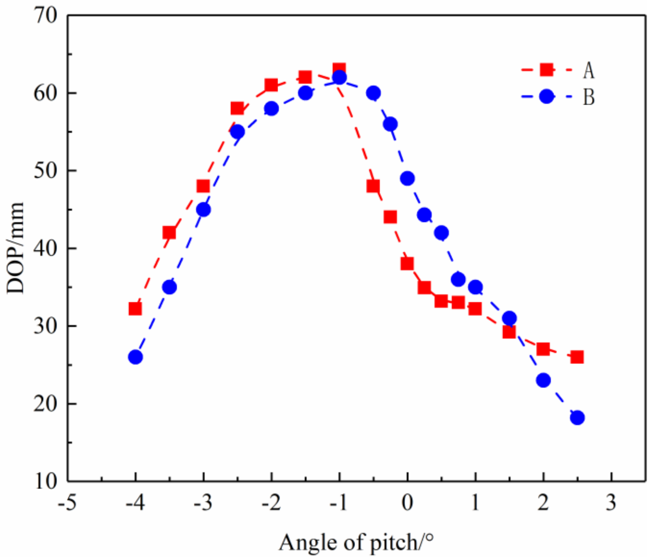

Figure 25. *Influence of impact attitude (angle of pitch) of long rod projectiles on penetration depth.*

Figure 25 illustrates the effect of the impact attitude (pitch) of long rod projectile on penetration depth when penetrating an oblique spaced target. The depth referred to the penetration thickness in the second layer of the target, with the first layer at an inclination of 60° and a thickness of 10mm, and the second layer being a Q235 steel plate at the same angle with a normal spacing of 5cm. The impact attitude of long rod projectile (defined such that an increase in the angle between the projectile axis and the target plate normal is positive and a decrease is negative) had a significant effect on the penetration results when penetrating a oblique target. As shown in Figure 25, it can be seen that a positive attack angle had an adverse effect on the penetration of long rod projectile, while a negative attack angle within the range of (-3° to 0°) produced a favorable effect on penetration. Specifically, Type-B projectiles achieved greater penetration depth than Type-A projectiles within the pitch angle range of (-1° to +1.5°), which was attributed to the previously mentioned thin-thick-thin structure of Type-A. When the impact attitude was at a positive attack angle, the mid-section of the projectile collided with the target, leading to a bending force on the penetrator core, which made it prone to breakage. Conversely, at a negative attack angle, after the head of the long rod projectile formed a crater, the subsequent thicker mid-section no longer contacted the target, making the penetrator core less prone to breakage, as seen in Figures 27-28. On the other hand, Type-B projectiles were less affected within the range of (-1° to +1.5°). However, when the angle exceeded +1.5°, Type-B experienced continuous erosion from the target due to the lack of protrusions on the mid-threaded section, exacerbating the deflection and erosion of the penetrator core, and thus reducing the penetration capability. When the angle ranges from -4° to -1°, both projectile types experienced reduced penetration due to the influence of the upper target plate on the penetrator core. Type-A had greater mass and kinetic energy, resulting in deeper penetration compared to Type-B.

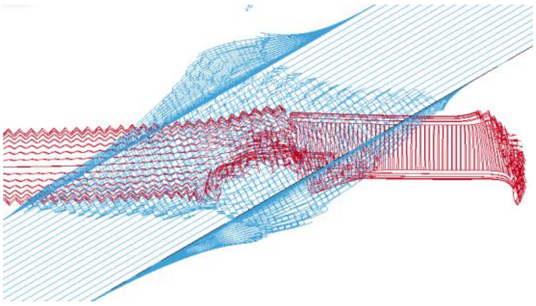

Figure 26. *Penetration state at a positive pitch angle.*

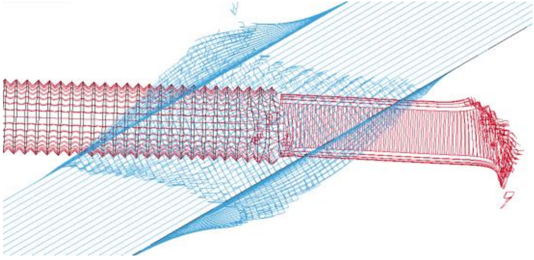

Figure 27. *Penetration state at a negative pitch angle.*

4.5 Influence of impact attitude (yaw angle) of long rod projectiles on penetration depth

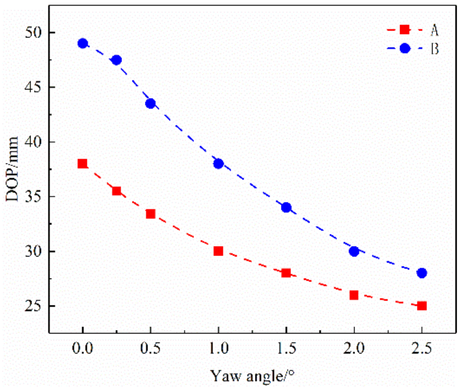

Figure 28. Influence of impact attitude (yaw angle) of long rod projectiles on penetration depth.

The target setup used to study the effect of yaw angle on penetration depth was the same as that for pitch angle. As seen in Figure 28, it is evident that the penetration capability of both projectile types was affected by the yaw angle; as the yaw angle increased, the penetration depth decreased. At the same angle, Type-B exhibited a higher penetration depth than Type-A and was less influenced by the yaw angle.

For Type-A penetrator cores with a pitch angle of attack, the target plate thickness required to induce projectile fracture decreased gradually with increasing impact velocity. Moreover, the decreasing trend became more gradual as the positive angle of attack increased (as shown in Figure 29). Within the conventional impact velocity range of 800-1800 m/s for rod-shaped armor-piercing projectiles, the critical target thickness necessary to cause projectile fracture generally did not exceed one projectile diameter.

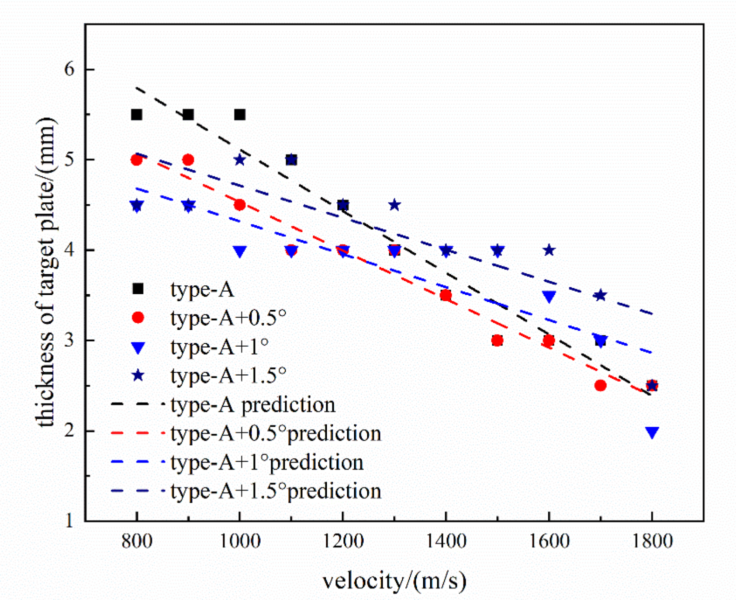

Figure 29. *Critical target thickness required for fracture initiation in Type-A penetrating at positive angles of attack.*

For Type-A cores impacting at negative angles of attack, the required target plate thickness exhibited similar patterns to positive angles at 0.5°. However, when the angle increased from 1°to 2.5°, the critical thickness remained nearly constant at impact velocities below 1600 m/s, followed by a sharp decrease once the velocity exceeded this threshold.

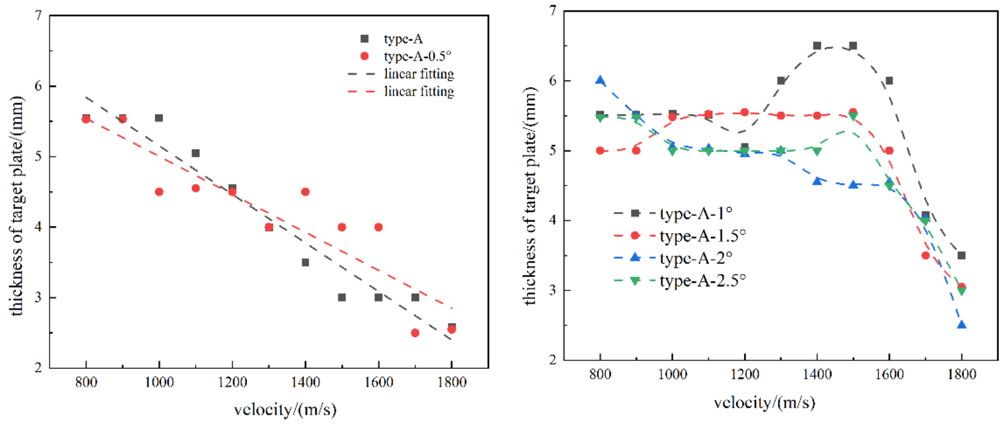

(a) (b)

Figure 30. *Critical target thickness for fracture initiation in Type-A penetrating at negative angles of attack.*

For Type-A impacting with yaw angles (0.5°–2.5°), the required target thickness to induce fracture (Figure 31) generally remained below one projectile diameter. A sharp decrease in critical thickness was observed when velocities exceeded 1400 m/s.

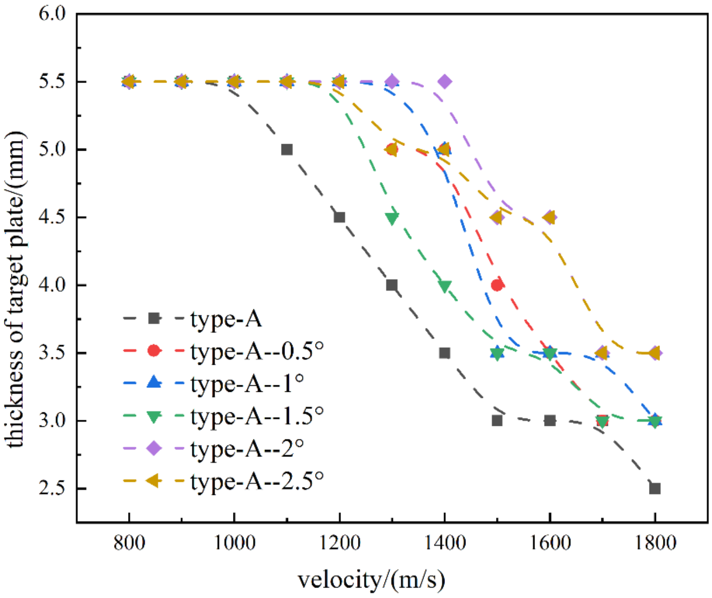

Figure 31. *Critical target thickness for fracture initiation in Type-A penetrating at yaw angles.*

To investigate size effects on fracture behaviour, Type-A and B were scaled while maintaining a constant length-to-diameter ratio. Two scaled configurations were tested: 24 mm (2× original length) and 48 mm (4× original length). As shown in Figure 32, the critical target thickness corresponding to fracture initiation is presented for six rod configurations across varying impact velocities. Type-A penetrator cores followed the established pattern where critical thickness rarely exceeded one diameter and decreased progressively with increasing velocity. Conversely, Type-B penetrator cores exhibited an inverse trend, particularly for the Type-B-48 variant, which showed significant thickness increase at higher velocities. The observed thickness increase for Type-B penetrator cores with rising velocities was attributed to velocity-dependent crater enlargement. Due to the absence of a reinforced protrusion at the midsection of Type-B, reduced mid-body contact with the expanding crater walls occurred, thereby delaying fracture initiation.

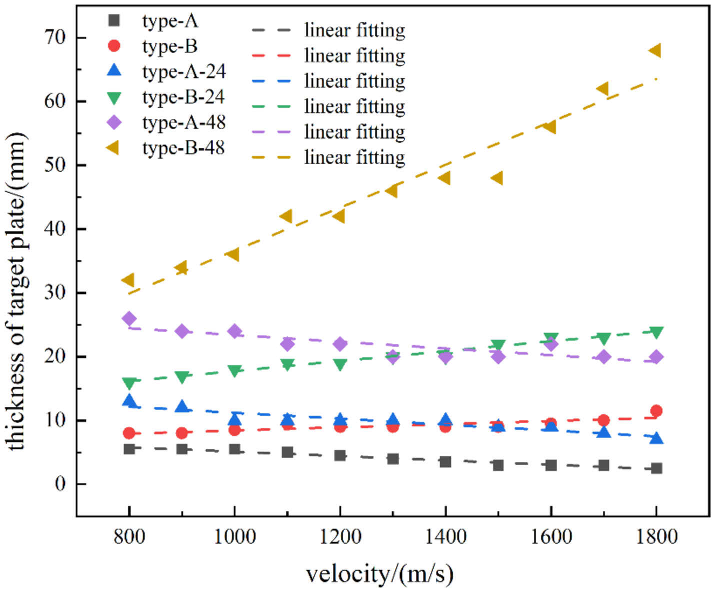

Figure 32. *Comparative critical target thickness for fracture initiation in scaled Type-A/B penetrator cores.*

4.6 The role of the sliding armor-piercing blocks and weakening grooves

Through the aforementioned research, it was found that when a tungsten alloy armor-piercing projectile with a large length-to-diameter ratio had a certain pitch or yaw angle, simply modifying the thin-thick-thin structure of penetrator core was not effective in dealing with oblique spaced targets. To reduce the impact of large-spaced targets with large angle of obliquity on the penetration capability of tungsten alloy long rod projectiles with a large length-to-diameter ratio, this study sought a solution to address the fracture mechanism of oblique targets on long rod projectiles (as shown in Figure 5), by modifying Type-A and B projectiles, and studying the penetration effect after installing the sliding armor-piercing blocks and weakening grooves (as shown in Figure 33) at the head of the penetrator core.

Figure 33. Nosed armor-piercing blocks and weakening grooves of penetrator core.

The working principle is as follows:

1) When the compression wave generated by the projectile head impacting the first layer of the target propagates backward, it encountered a step structure with an increasing cross-section, causing attenuation of the transmitted compression wave.

2) The armor-piercing blocks were attached together and pressed onto the projectile body by the wind cap, with little to no tensile or shear force between them. In the early stages of impacting the target, the target resistance was aligned with its normal direction, causing the armor-piercing blocks to experience radial resistance components, which gave them a radial movement tendency. Since the armor-piercing blocks could slide relatively, this radial movement tendency did not or rarely transfers to the projectile body, reducing the tendency of the projectile to jump.

3) Due to the relative sliding of the armor-piercing blocks, the crater size they form on the first layer target could be increased, opening up a path for the subsequent projectile body to advance and to minimize the disturbance when the projectile passed through the first layer target.

4) After penetrating the first layer target, the armor-piercing blocks detach from the projectile body, thereby controlling the loss of projectile head mass and ensuring the penetration capability against subsequent target.

5) During the penetration of multi-layer thin targets, the nosed armor-piercing blocks would detach from the main body of penetrator core, relying on the weakening grooves to cause active fracture of penetrator core and reduce the

disturbance from the targets. This also applied to penetrating thicker targets, where the active fracture of penetrator core similarly reduced the disturbance from the targets.

To verify the effectiveness of the simulation design, the original diameter of the weakening grooves was reduced from 5.6mm to 4.1mm, and other parameter settings were the same as when penetrating the three-layer target in the previous parts. The results are shown in Figure 34 (compared to Figure 19), indicating that this structure could effectively reduce the impact of multi-layer spaced targets on long rod projectiles.

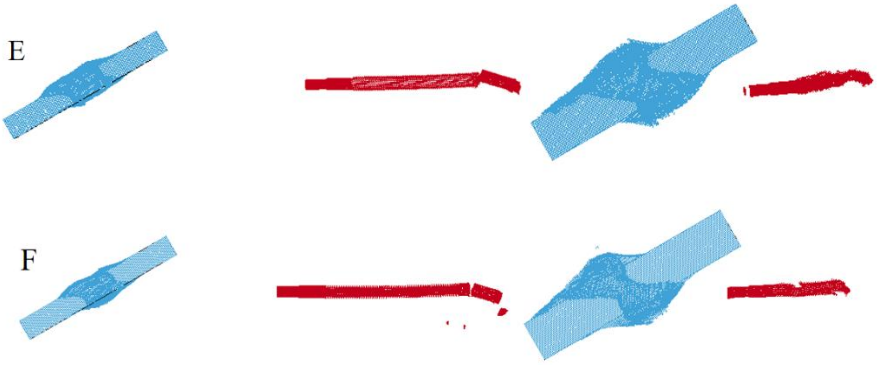

Figure 34. *Simulation results of Type-E and F projectiles.*

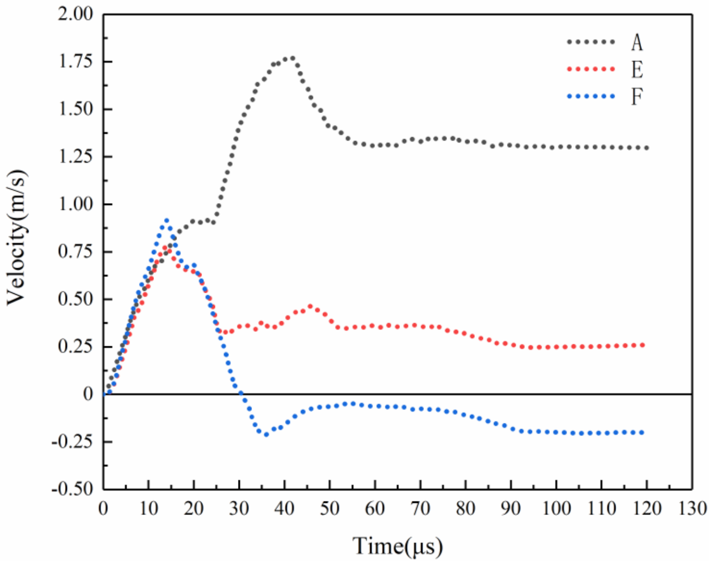

Figure 35. *Deflection speed changes of Type-A, E, and F projectiles.*

Figure 35 illustrates the deflection velocity changes of three projectile types after penetrating the first layer target. It is evident that Types-E and F could reduce the deflection velocity of the penetrator core, indicating that the change in the penetration attitude of penetrator core was smaller, and it could maintain better penetration capability. Specifically, Type-F projectile caused the penetrator core to develop a downward velocity, equivalent to generating a negative pitch angle. From the results after penetrating the second layer target, Type F projectile exhibited a better attitude, and the penetrator core remains more intact. By changing the core structures of tungsten alloy long rod projectiles with a large length-to-diameter ratio, the influence of large-spaced targets with large angle of obliquity on penetration performance of the projectiles could be reduced.

5 Conclusion

This study conducted experiments on the tungsten alloy long rod projectiles with large length-to-diameter ratio penetrating the single-layer, double-layer spaced and three-layer spaced Q235 steel targets at a 60°angle of obliquity. High-speed laser photography was employed to observe the penetration process of pennetrator core, and the fractured pennetrator core recovered after penetration were analyzed. The J-C constitutive parameters of the 93W alloy were obtained through mechanical tests, and a series of simulation studies were conducted. The following conclusions were drawn regarding the influence of spaced targets with large angle of obliquity on the penetration performance of tungsten alloy rod projectiles with a large length-to-diameter ratio :

1) The mechanism by which spaced targets with large angle of obliquity affect tungsten alloy rod projectiles with large length-to-diameter ratio was by causing trajectory deflection and projectile body fracture. The fracture pattern predominantly involved transgranular failure and W grain fragmentation, exhibiting negligible deformation. Spaced targets with large angle of obliquity could significantly reduce the penetration performance of tungsten alloy rod projectiles.

2) The J-C constitutive parameters of the 93W alloy obtained from mechanical tests were validated through simulations, showing small deviation from the experimental results.

3) When penetrating the large-angle steel targets without an angle of attack, reducing the length-to-diameter ratio of penetrator core couldn't effectively prevent the fracture of the thin-thick-thin structure of long rod projectiles.

4) As the angle of the oblique targets increased, the required target thickness for causing fracture of the tungsten alloy long rod projectile gradually decreased. Reducing the diameter of the middle-threaded section could enhance the fracture resistance of the tungsten alloy long rod projectiles. As the spacing of the oblique targets increased, the penetration depth of the long rod projectile showed a fluctuating downward trend.

5) Changing the structure of the tungsten alloy long rod projectiles from thin-thick-thin to thin-thin-thin could reduce the influence of spaced targets with large angle of obliquity on the penetration performance of long rod projectiles when the projectiles had the angle of attack (pitch and yaw) and the pitch angle was within the range of (-1° to +1.5°) and the yaw angle was within the range of (0° to +2.5°).

6) By changing the thin-thick-thin structure of the tungsten alloy long rod projectile, setting up armor-piercing blocks, and adding weakening grooves to induce active fracture of the penetrator core, the attitude of the penetrator core after penetrating the spaced targets with large angle of obliquity was effectively maintained, thereby reducing the influence of spaced targets with large angle of obliquity on the penetration performance of tungsten alloy long rod projectiles with large length-to-diameter ratio.

Author's contributions:

Data availability:

Editor: Marcílio Alves

References

G.Z. Zhao. Armor-piercing Engineering Mechanics. Beijing: Ordnance Industry Press;1992.

W.B. Li, P.H. Shen, X.M. Wang, et al. Experimental study on secondary fragment dispersion of projectile inclined impact on target plate. Journal of Nanjing University of Science and Technology (Natural Science Edition) 2002; 03:263-66.

Charles E. Anderson, James D. Walker, Stephan J. Bless, et al. On the velocity dependence of the L/D effect for long-rod penetrators, Int J Impact Eng 1995; 17(1–3):13-24.

Charles E. Anderson, James S. Wilbeck, Jeffrey S. Elder, Long-rod penetration into highly oblique, water-filled targets, Int J Impact Eng 1995; 23, (1-1):1-12.

Hohler V, Rothenhausler H, schneider E, Untersuchung der Shockwirkung auf Panzerfahrzeuge. Ernst Mach Institute Report No.V2/78(in German),mar 1978.

Y. Vayig, Z. Rosenberg, The effect of yaw on the penetration of rigid rods, Int J Impact Eng, 2021;148,103748.

Zvi Rosenberg, Roman Kositski, The hole diameter in metallic plates impacted by hypervelocity projectiles, Int J Impact Eng 2017;102: 147-155.

A.J. Stilp, K. Weber, Debris clouds behind double-layer targets, Int J Impact Eng, 1997; 20(6-10): 765-78.

V. Hohler, A.J. Stilp, K. Weber, Hypervelocity penetration of tungsten sinter-alloy rods into aluminum, Int J Impact Eng 1995; 17(1–3) 409-418.

S. Chocron, C.E. Anderson, J.D. Walker, et al. A unified model for long-rod penetration in multiple metallic plates, Int J Impact Eng 2023;28(4): 391-411.

M.A. Iqbal, K. Senthil, V. Madhu, N.K. Gupta. Oblique impact on single, layered and spaced mild steel targets by 7.62 AP projectiles, Int J Impact Eng 2017; 110:26-38.

K. Senthil, M.A. Iqbal, Effect of projectile diameter on ballistic resistance and failure mechanism of single and layered aluminum plates, Theoretical and Applied Fracture Mechanics 2013;67–68:53-64.

J.A Zukas, D.R Scheffler. Impact effects in multilayered plates, International Journal of Solids and Structures 2001; 38(19): 3321-28.

E.A. Flores-Johnson, M. Saleh, L. Edwards. Ballistic performance of multi-layered metallic plates impacted by a 7.62-mm APM2 projectile, Int J Impact Eng 2011;38(12): 1022-32.

M.A. Iqbal, K. Senthil, V. Madhu, N.K. Gupta. Oblique impact on single, layered and spaced mild steel targets by 7.62 AP projectiles, Int J Impact Eng 2017;110: 26-38.

Zaid Mohammad, P.K. Gupta, M.A. Iqbal, et al. Energy Absorption in Metallic Targets Subjected to Oblique Impact, Procedia Engineering 2017;173: 145-52.

P.K. Gupta, M.A. Iqbal, Zaid Mohammad, et al. Energy absorption in thin metallic targets subjected to oblique projectile impact: A numerical study, Thin-Walled Structures 2018;126: 58-67.

P. K. Gupta, M. A. Iqbal, Zaid Mohammad. Energy dissipation in plastic deformation of thin aluminum targets subjected to projectile impact, Int J Impact Eng 2017; 110: 85-96.

Zaid Mohammad, Pramod Kumar Gupta, Abdul Baqi, Experimental and numerical investigations on the behavior of thin metallic plate targets subjected to ballistic impact, Int J Impact Eng 2020:146; 103717.

Y Deng, W Zhang, Z Cao. Experimental investigation on the ballistic resistance of monolithic and multi-layered plates against hemispherical-nosed projectiles impact, Materi Des 2012;41: 266-81.

Y. Deng, W. Zhang, Z Cao. Experimental investigation on the ballistic resistance of monolithic and multi-layered plates against ogival-nosed rigid projectiles impact, Mater Des, 2013; 44: 228-39.

W. Zhang, Y. F. Deng, Z. S. Cao, et al. Experimental investigation on the ballistic performance of monolithic and layered metal plates subjected to impact by blunt rigid projectiles, Int J Impact Eng., 2012;49: 115-29.

S. Dey, T. Børvik, X. Teng, et al. On the ballistic resistance of double-layered steel plates: An experimental and numerical investigation, International Journal of Solids and Structures., 2007;44(20): 6701-23.

T Børvik, M Langseth, O.S Hopperstad, et al. Perforation of 12mm thick steel plates by 20mm diameter projectiles with flat, hemispherical and conical noses: Part I: Experimental study, Int J Impact Eng 2002; 27 (1): 19-35.

T. Børvik, O.S. Hopperstad, T. Berstad, et al. Perforation of 12mm thick steel plates by 20mm diameter projectiles with flat, hemispherical and conical noses: Part II: numerical simulations, Int J Impact Eng 2002; 27 (1): 37-64.

Zaid Mohammad, Pramod Kumar Gupta, Abdul Baqi. Ballistic performance of monolithic and double layered thin-metallic hemispherical shells at normal and oblique impact, Thin-Walled Structures 2021; 159: 107257.

J. Awerbuch, S.R. Bodner. An investigation of oblique perforation of metallic plates by projectiles. MED Report No. 48, Material Mechanics Laboratory, Department of Materials Engineering, TECHNION, Israel Institute of Technology, Haifa, Israel Exp Mech 1977;17: 147-153.

V. Madhu, T.B. Bhat, NK Gupta. Normal and oblique impacts of hard projectile on single and layered plates-an experimental study, Defence Sci 2003; 53 (2): 147-56.

D.W. Zhou, W.J. Stronge. Ballistic limit for oblique impact of thin sandwich panels and spaced plates, Int J Impact Eng 2008; 35 (11): 1339-54.

M. A. Iqbal, G. Gupta, N.K. Gupta. 3D numerical simulations of ductile targets subjected to oblique impact by sharp nosed projectiles, Int J Impact Eng 2010; 47: 224-237.

M.A. Iqbal, S.H. Khan, R. Ansari, et al. Experimental and numerical studies of double-nosed projectile impact on aluminum plates, Int J Impact Eng 2013;54: 232-45.

Z Mohammad, PK Gupta, MA Iqbal, A Baqi Energy absorption in metallic targets subjected to oblique impact Procedia Eng 2017;173: 145-52.

PK Gupta, MA Iqbal, Z Mohammad. Energy dissipation in plastic deformation of thin aluminum targets subjected to projectile, Int J Impact Eng 2017;110: 85-96.

X. Teng, T. Wierzbicki, M. Huang. Ballistic resistance of double-layered armor plates, Int J Impact Eng 2008;35(8): 870-84.

X.Z. Tang, Z.J. Wang, L. Y. Dong, et al. Numerical simulation of Projectile Oblique Impact on spaced target plate, Journal of Ordnance Equipment Engineering 2019;40(06):47-50.

Y. Long, X. b. Yue, X. Zhou, et al. Study on the penetration characteristics of high-speed steel bullets on multi-layer large-spaced metal targets, Journal of Nanjing University of Science and Technology (Natural Science Edition) 2004; 04: 369-74.

R.Y. Zhao, H.Y. LU, M. Zhu. Numerical Simulation of rod-type kinetic vehicle penetrating multi-layer target. Journal of Projectiles, Arrows and Guidance 2012;32(06):96-98+116.

M.A. Iqbal, K. Senthil, V. Madhu, N.K. Gupta, Oblique impact on single, layered and spaced mild steel targets by 7.62 AP projectiles, Int J Impact Eng 2017;110: 26-38.

Y. N. Yuan, J. Hu, S.L. Wang, et al. Numerical Simulation and experiment of Tungsten Alloy Long rod projectile Oblique Penetration of spaced Target, Sichuan Ordnance Engineering Journal 2011;32(07):10-15.

Y.X. Dong, S.S. Feng, X.J. Duan. Research on characteristics of projectile oblique penetrating multi-layer metal spaced target, Journal of North University of China (Natural Science Edition) 2010;31(03):221-26.

J.Q. LI, T.S. LIU. Numerical simulation of rod-resistant elastic energy of double-spaced target, Journal of Ballistic and Guidance 2009;29(05): -149151.

Jinxin Pan, Qing Peng, Xiaoming Liu, Yueguang Wei, Impact fracture of brittle plate, International Journal of Solids and Structures, 2025,311 113249.

C. Sénac, Mechanisms and micromechanics of intergranular ductile fracture, International Journal of Solids and Structures, 2024,301, 112951.

Maziar Khademi, Mohammad Javad Mirnia, Hassan Moslemi Naeini, Numerical analysis of ductile fracture in stretch bending of AA6061-T6 aluminum alloy sheet using GTN damage model, International Journal of Solids and Structures, 2024,301, 112947.

H. Chang, Y.B. Dong, W. Setyawan, et al. Effect of radiation defects on grain boundary evolution under shock loading, Journal of Materials Research and Technology, 2024, 301,698-707.

H. Gietl, S. Olbrich, J. Riesch, et al. Estimation of the fracture toughness of tungsten fibre-reinforced tungsten composites, Engineering Fracture Mechanics, Volume ,2020,232,107011.

H. Safahi, M.R. Sabour,G. Faraji, et al. Fracture behavior of W-20Cu composite processed via copper melt infiltration into tungsten wire skeleton, Engineering Failure Analysis, 2025,107, 109426.

G. X. Yin, W. B. Li, et al. Study of armor-piercing self-sharpening properties of 88WC-12Co material Ballistic performance, (2022 ICDT) 2478 (2023) 072006.

JOHNSON G R, COOK W H. A constitutive model and data for metals subjected to large strains, high strain rates and high temperatures. Proceedings of the 7th International Symposium on Ballistics. Hague, the Netherlands: IBC, 1983; 541-47.

F. l. Zhu, Y. Chen, G. l. Zhu, Numerical simulation study on penetration performance of depleted Uranium (DU) alloy fragments, Defence Technology 2021;17(1): 50-55.